Predictions of x-ray scattering spectra for warm dense matter

A. N. Souza,[1] D. J. Perkins,[2] C. E. Starrett,[3,*] D. Saumon,[3] and S. B. Hansen[4]
[1]*Department of Mathematics, University of Michigan, Ann Arbor, Michigan 48019, USA*
[2]*Department of Physics and Astronomy, University of California, Los Angeles, California 90095, USA*
[3]*Los Alamos National Laboratory, P. O. Box 1663, Los Alamos, New Mexico 87545, USA*
[4]*Sandia National Laboratories, P. O. Box 5800, Albuquerque, New Mexico 87185, USA*
(Received 6 November 2013; revised manuscript received 28 January 2014; published 24 February 2014)

We present calculations of x-ray scattering spectra based on ionic and electronic structure factors that are computed from a new model for warm dense matter. In this model, which has no free parameters, the ionic structure is determined consistently with the electronic structure of the bound and free states. The x-ray scattering spectrum is thus fully determined by the plasma temperature, density and nuclear charge, and the experimental parameters. The combined model of warm dense matter and of the x-ray scattering theory is validated against an experiment on room-temperature, solid beryllium. It is then applied to experiments on warm dense beryllium and aluminum. Generally good agreement is found with the experiments. However, some significant discrepancies are revealed and appraised. Based on the strength of our model, we discuss the current state of x-ray scattering experiments on warm dense matter and their potential to determine plasma parameters, to discriminate among models, and to reveal interesting and difficult to model physics in dense plasmas.

DOI: 10.1103/PhysRevE.89.023108 PACS number(s): 52.25.Os, 52.38.−r, 52.27.Gr

I. INTRODUCTION

Warm dense matter (WDM) refers to plasmas of roughly solid density with temperatures of ∼1 to 10^2 eV. Because few of the simplifying limits applicable to classical plasma and condensed matter physics can be used in the WDM regime, it is difficult to model. And while transient WDM states occur in many dynamic experiments, its opacity makes it difficult to probe experimentally. X-ray scattering has become an important diagnostic of WDM in the past decade [1–6]; however, only recently have the models used to diagnose WDM been tested against high-quality data from experiments with cold materials [7]. This benchmarking has revealed some underlying problems with widely used scattering models [8]. Understanding the properties of WDM is important for planetary research [9], modeling dense stars such as white dwarfs [10], and for inertial confinement fusion [11]. In this paper we calculate x-ray scattering spectra from a new model of WDM that is based on a unified approach in which all necessary plasma properties are calculated consistently.

Our approach uses the model of Refs. [12,13],[1] which improves on the formalism of Ref. [14] to calculate the electronic structure (bound and free states) as well as the ionic structure of the plasma. The model [12] combines an average atom model based on density functional theory (DFT) to compute the electronic structure of the plasma with the integral equations of fluid theory for the ion interactions, enabling an efficient calculation of the plasma properties. The inputs to the model are the plasma mass density, temperature, and the species (nuclear charge and mass). For a given choice of exchange and correlation potential, there are no adjustable parameters. The model then gives the ion-ion and ion-electron interaction potentials, the ion pair distribution function, the bound and continuum wave functions, bound state energies, density of states, ionization fraction, and naturally accounts for resonances and pressure ionization, all calculated self-consistently. The ionic pair distribution functions have been shown to agree very well with *ab initio* simulations [12,13] over a wide range of atomic numbers and plasma conditions.

Using the outputs from this model, we calculate x-ray scattering spectra using the Chihara formalism [15] (Sec. II) which is based on a chemical picture of the plasma in which there are well-defined ions, whose bound electrons are clearly separated from the continuum electrons. In this context, the scattering spectrum is the sum of three components: elastic, bound-free, and free-free. The elastic component is calculated from the static ion-ion structure factor and the density of those electrons which move with the ion, all of which are computed from the model of Ref. [12]. We calculate the bound-free component with the approach proposed by Johnson *et al.* [16], using the bound and free wave functions from the model of Ref. [12]. Finally, for the free-free component we use both the RPA [17] and the Born-Mermin (BM) approximation to account for ion-electron coupling [18–20] and compare the results.

We first validate our approach (Sec. III) with a comparison to an x-ray scattering experiment on solid beryllium at ambient conditions [7] (hereafter referred to as the "cold Be" experiment), for which the target conditions and energy-resolved intensity profile of the x-ray probe are accurately known and controlled. Though the model [12] is primarily designed for plasmas, the comparison with this experiment validates the overall implementation and also gives insights into the limitations of the approximations used.

We then compare to x-ray scattering experiments on warm dense beryllium [4] (Sec. IV) and aluminum [6] (Sec. V). In contrast to the cold Be experiment, these experiments are more technically challenging, resulting in weaker, noisier signals and possibly uncontrolled systematic effects in the scattered spectrum. We consider the effects on the scattered spectrum of variations in density and temperature as well as uncertainties in the x-ray source spectrum. Some points of disagreement with the experimental data are found and discussed.

*starrett@lanl.gov
[1]Specifically we use the QM-IS model of Ref. [13].

In Sec. VI we present an x-ray scattering spectrum for warm dense Be in a hypothetical experiment. We assume the same target conditions as in the experiment [4] but use the x-ray probe parameters from the cold Be experiment [7]. Comparing these spectra to the spectra from the cold Be experiment reveals the effects of increased temperature and density and the experimental requirements to detect them. In Sec. VII, an example of an x-ray scattering spectrum for a higher Z element (Ti) highlights resonant features whose experimental characterization is of interest to constrain models of WDM. Finally, we review our analysis of these experiments with our predictive model for x-ray scattering spectra and comment on the experimental requirements to constrain models of WDM.

II. THEORY

In x-ray scattering experiments in WDM, a beam of probe x rays with a known spectral intensity profile scatters off a WDM sample and the x rays are collected at a fixed scattering angle θ, and their spectral intensity profile measured. The scattering is described by the dynamic structure factor $S(k,\omega)$, where [18][2]

$$k = 2k_0 \sin\left(\frac{\theta}{2}\right) \tag{1}$$

is the magnitude of the momentum transfer to the photon. $\vec{k} = \vec{k}_1 - \vec{k}_0$, where $\vec{k}_0$ and $\vec{k}_1$ are the initial and final photon wave numbers, respectively, and $\omega = \omega_0 - \omega_1$ is the energy transfer to the electron. Chihara [15] has shown that by assuming a clear distinction between bound and free electrons, $S(k,\omega)$ can be written as the sum of three terms as follows:

$$S(k,\omega) = \underbrace{|f_I(k) + q(k)|^2 S_{ii}(k,\omega)}_{\text{elastic}} + \underbrace{\bar{Z} S_{ee}(k,\omega)}_{\text{free-free}} + \underbrace{S_{bf}(k,\omega)}_{\text{bound-free}}. \tag{2}$$

This expression is the basis of nearly all theoretical calculations of x-ray scattering spectra of WDM after various approximations have been applied to each of the three terms [8,16,18,21]. The essence of the present contribution is that Eq. (2) is evaluated with a self-consistent model of the electronic and ionic structures of the plasma.

The *elastic* component is due to photons elastically scattered by electrons that follow the motion of the ions. Due to their large mass, the dynamic structure factor of the ions $S_{ii}(k,\omega)$ is a very narrow feature in frequency. While it is rich in information regarding ion dynamics [22], it can be suitably approximated as $S_{ii}(k,\omega) = S_{ii}(k)\delta(\omega)$ for our purposes as it is not resolved in the experiments considered here. In the language of the model [12] the electrons that follow the ion motion are described by the pseudoatom electron density $n_e^{\rm pa}(r)$ which can be split into bound (ion) and free (screening) components, $n_e^{\rm ion}(r)$ and $n_e^{\rm scr}(r)$. The quantities $f_I(k)$ and $q(k)$ are the Fourier transforms of $n_e^{\rm ion}(r)$ and $n_e^{\rm scr}(r)$, respectively. These, together with the ion-ion structure factor $S_{ii}(k)$, are all determined within the model [12] without further approximation.

The *free-free* component describes scattering from free electrons which can be calculated using the random-phase approximation (RPA). The RPA treats the free electrons as a collisionless plasma, a questionable approximation in the WDM regime [8]. Nevertheless it has been widely used to model WDM x-ray experiments [16,18,23] with apparent success.

In the RPA approximation the free-free component is a function only of the free electron density $\bar{n}_e^0$, the average ionization $\bar{Z}$, and the temperature T. $\bar{n}_e^0$ and $\bar{Z}$ are determined in the model [12] for the given plasma conditions (temperature, mass density, and nuclear charge). The ion charge $\bar{Z}$ is defined as the number of positive energy electrons per nucleus and is intrinsically linked to the determination of the ion structure.

It is possible to extend the RPA with the Born-Mermin (BM) approximation to include the effects of electron-ion collisions in a perturbative way [18,19]. In addition to its dependence on $\bar{n}_e^0$, $\bar{Z}$, and T, this approximation requires a knowledge of the dynamical electron-ion collision frequency, which is calculated in the Born approximation [18],

$$\nu^B(\omega) = \frac{-i}{24\pi^3\bar{Z}} \int_0^\infty dk\, k^6 \left[V_{ie}^S(k)\right]^2 S_{ii}(k) \frac{1}{\omega} \times \left[\epsilon_e^{\rm RPA}(k,\omega) - \epsilon_e^{\rm RPA}(k,0)\right], \tag{3}$$

where $\epsilon_e^{\rm RPA}$ is the RPA dielectric function [24] and V_{ie}^S is the statically screened electron-ion interaction potential. In the notation of the model [12]

$$\beta V_{ie}^S(k) = \frac{-C_{Ie}(k)}{\epsilon_e^{\rm RPA}(k,0)}, \tag{4}$$

where $-C_{Ie}(k)/\beta$ is the Fourier transform of the electron-ion pseudopotential, which is determined within the model.

The dimensionless scattering parameter α provides a distinction between two regimes in $S_{ee}(k,\omega)$ and is given by $\alpha = k_{\rm scr}/k$ [18] where $k_{\rm scr}$ is the screening wave vector,

$$k_{\rm scr}^2 = 2\pi\beta n_e \frac{I_{-1/2}(\eta)}{I_{1/2}(\eta)}, \tag{5}$$

I_n is the Fermi integral of index n, $\beta = 1/kT$, $\eta = \beta\mu_{\rm e}$ is the dimensionless chemical potential of the electrons, and n_e is the (average) free electron density. This expression for $k_{\rm scr}$ recovers the Thomas-Fermi screening length at $T = 0$ and the Debye screening length at high T. Collective scattering of the x rays occurs for $\alpha \gg 1$, where the free electrons can screen the relatively slow density oscillations caused by the x-ray electromagnetic waves. For $\alpha \ll 1$, x rays are scattered noncollectively by electrons whose density is essentially "frozen" over the period of the wave. Based on finite-temperature quantum molecular dynamics calculations to obtain a realistic estimate of the electron-ion collision frequency $\nu^B(\omega)$, the authors of Ref. [25] found that the BM approximation is poor for $\alpha > 1$ but becomes quite reasonable in the noncollective regime ($\alpha < 1$) and improves as α decreases. As we will see below, the BM approximation and the RPA are nearly identical for $\alpha \lesssim 0.5$. We can expect the RPA (and its BM extension) to give a good approximation

[2]Unless otherwise noted, we have used atomic units throughout, with $\hbar = m_e = k_B = e = 1$, where the symbols have their usual meaning.

to $S_{ee}(k,\omega)$ in the noncollective regime. The convolution of the free-free feature with a relatively broad probe beam (experimentally, a width comparable to the plasmon frequency is not uncommon) can largely mask the difference between the RPA and more accurate calculations of $S_{ee}(k,\omega)$ for values of α relevant to warm dense matter.

Finally, the *bound-free* component of the dynamical structure factor describes inelastic scattering from bound electrons which are photoionized in the process. This is determined from matrix elements between bound and continuum wave functions following the formulation of [16]

$$S_{bf}(k,\omega) = \sum_{n\ell} \frac{4(2\ell+1)p}{\pi} \mathcal{F}(\epsilon_{n\ell})(1-\mathcal{F}(\epsilon))M(\epsilon_{n\ell}) \times \sum_{\ell_1\ell_2} A_{\ell_1\ell\ell_2} \left| I_{\ell_1\ell\ell_2}(p,k) \right|^2 \quad (6)$$

$$I_{\ell_1\ell\ell_2}(p,k) = \frac{1}{p}\int_0^\infty P_{\epsilon\ell_1}(r) j_{\ell_2}(kr) P_{n\ell}(r) \sqrt{f^{\rm cut}(r)}\, dr, \quad (7)$$

where $\mathcal{F}$ is the Fermi-Dirac occupation factor, $\epsilon = p^2/2$ is the energy of the continuum electron state, and ϵ_{nl} is the energy of the bound state of orbital angular momentum ℓ and principal quantum number n. $P_{n\ell}$ and $P_{\epsilon\ell}$ are the radial wave functions [16] of the bound (initial) and continuum (final) states, respectively, j_ℓ is the spherical Bessel function of index ℓ, and

$$A_{\ell_1\ell\ell_2} = (2\ell_1+1)(2\ell_2+1)\begin{pmatrix} \ell_1 & \ell & \ell_2 \\ 0 & 0 & 0 \end{pmatrix}^2, \quad (8)$$

where $\begin{pmatrix} \ell_1 & \ell & \ell_2 \\ 0 & 0 & 0 \end{pmatrix}$ is the Wigner 3-J symbol. All radial wave functions are produced by our model of WDM [12].

This expression differs from Eq. (22) of Ref. [16] as we include the unoccupied fraction of the final state $1-\mathcal{F}(\epsilon)$ [8]. The factors $M(\epsilon_{n\ell})$ and $f^{\rm cut}(r)$ are integral to the definition of the ion electron density that ensures continuity as a bound state crosses into the continuum [12]. The first of these factors, $M(\epsilon_{n\ell})$, is a partial occupation factor for weakly bound states that are not well separated in energy from the continuum states. The second, $f^{\rm cut}$, limits spatially the ion electron density of weakly bound states that can otherwise extend to several times the ion sphere radius [12]. We stress that $M(\epsilon_{n\ell})$ and $f^{\rm cut}(r)$ affect only weakly bound states whose contributions to x-ray scattering from the theory of Chihara (2) are uncertain since those bound electrons are not clearly distinguishable from those in the continuum. In regimes where the bound and continuum states are well separated, $M(\epsilon_{n\ell})$ and $f^{\rm cut}(r)$ have no effect. Last, we note that the bound and free wave functions appearing in Eq. (7) are orthogonal by construction, which has been demonstrated to be an important property for such calculations [26].

Comparisons with experimental data require that the theoretical spectrum given by Eq. (2) be convolved with the spectral distribution of the incident x-ray photons [18]. Since the ion elastic feature is modeled as a δ function in frequency, the calculated elastic feature takes the shape of the incident x-ray energy profile. Finally, all the calculations presented here assume thermal equilibrium between ions and electrons ($T_e = T_i = T$), although this is not an intrinsic limitation of our model.

III. COLD SOLID BERYLLIUM

In order to validate these approximations and our overall approach, we compare our calculations to an x-ray scattering experiment on solid Be at normal conditions (Fig. 1) [7] that probe the bound-free and free-free terms in Eq. (2). In this experiment a very narrow x-ray probe with a Gaussian profile [1.3-eV full width at half maximum (FWHM)] scattered from the cold Be target and photons were collected at several

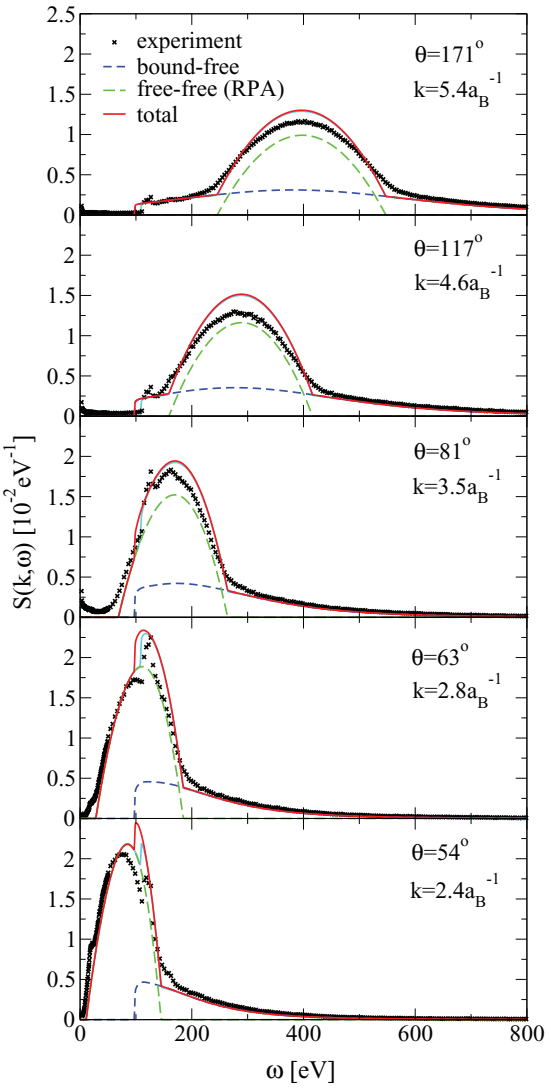

FIG. 1. (Color online) Comparison of theoretical x-ray scattering spectra with an experiment on solid beryllium at ambient conditions [7]. "Total" corresponds to the sum of the bound-free and free-free terms, calculated with the Dirac exchange functional. The solid cyan (light gray) line is the total using Slater exchange in the calculation of bound and free electronic states. It is mostly indistinguishable from the calculation using Dirac exchange except near the bound-free threshold, which is shifted slightly to the right. Note that to match the presentation of the data in Ref. [7], the frequency axis is reversed from the convention used in WDM experiments and in Figs. 3–5 and 7 (here $\omega = \omega_0 - \omega_1$).

scattering angles and at an energy of 9890 eV. The energy of the incident beam was varied to scan the energy range seen in Fig. 1. This introduces an additional weak k dependence in the spectrum as the energy is varied for each scattering angle [Eq. (1)]. We have ignored this and used the fixed k values given in Refs. [7,8] to generate the theoretical spectra. The model [12] cannot be applied directly at the experimental conditions where the Be is solid since it assumes a fluid structure. However, the narrow Bragg peaks of $S_{ii}(k)$ in the solid material ensure small elastic contributions to the scattering signal at most k values. The inelastic scattering is dependent primarily on the electronic properties, which do not vary significantly when T is much less than the Fermi temperature (14.3 eV for ambient Be). We have verified that solutions for solid density Be at $T = 0.1$ eV and 0.2 eV show no significant change in the bound-free and free-free contributions, indicating convergence with respect to temperature. It is therefore possible to make a meaningful comparison with this experiment. Note that the data have been normalized to calculations of the spectra with the method of real-space Green's function [7] of the electronic structure which effectively provide an absolute calibration of the data. We can thus compare our own calculations of the spectrum directly with this normalized data. Given the excellent agreement of the theory of Ref. [7] with the data, this also allows a direct comparison of two independent theories.

Using the Dirac exchange potential [27]

$$V_{\rm exch}(r) = -\left[\frac{3n_e(r)}{\pi}\right]^{1/3} \tag{9}$$

to compute the electronic states, our model predicts one bound state ($1s$) under these conditions with an energy of -86.1 eV with respect to the lowest continuum state. On the other hand, Fig. 1 shows that the calculated threshold for the bound-free term is $\omega = 98.0$ eV. The difference is due to the occupation of continuum states, which shifts the threshold to the first unoccupied state at the top of the Fermi sea. The shift is given by the electron chemical potential (11.9 eV).[3] In Fig. 1 it is seen that the experiment finds the bound-free threshold at $\sim$113 eV. The difference of 15 eV with our calculation is largely due to the DFT treatment of the electrons in the model. It is well known that the DFT systematically underestimates the binding energy of bound states by an amount that depends on the choice of exchange-correlation functional. One should not expect the simple Dirac functional to give very accurate results. This can be illustrated by replacing the Dirac functional with the Slater functional [28],[4] which, for all its simplicity, gives better predictions of the bound state energies. The result is shown in Fig. 1 as the solid cyan (light gray) line which lies directly under the Dirac exchange calculation labeled "total" (solid dark gray line) except near the bound-free threshold. The Slater exchange calculation gives a threshold energy of 107 eV, in better agreement with the experimental value and improving the agreement with the corresponding jump in $S(k,\omega)$. Away from the threshold, both functionals lead to very similar results and recover the long range bound-free tail quite well. Except for the position of the threshold, our calculation of the bound-free contribution is in very good agreement with the real-space Green's function calculation of Ref. [8].

For the free-free contribution we show only the RPA calculation in Fig. 1. The BM approximation depends strongly on the ionic structure factor $S_{ii}(k)$ [Eq. (3)] which we are unable to calculate for a solid with our model. We find that the RPA free-free contribution is in reasonable agreement with the experiment for all scattering angles probed in the experiment. However, it is systematically too narrow at its base and too high at its peak (by 5–20%). This is consistent with the calculations of Ref. [26], who also show that the BM approximation differs little from the RPA in this regime. Furthermore, the fact that the RPA works fairly well in this strongly noncollective regime ($\alpha = 0.21$–0.48 in this experiment) agrees very well with the results of Ref. [25]. The limitations of the RPA are highlighted by the high spectral resolution of this experiment (1.3 eV). In warm dense matter experiments, where the resolution is typically $\sim$100 eV or more, these small differences would be invisible.

Overall, the agreement of our model with this experiment is good, bearing in mind that the model [12] is not designed for solids but for plasmas. Systematic deviations with the experiment and with a more accurate theory developed for cold solids [7] are well understood and can be quantified to a good extent. With these caveats, this validates our theoretical approach to the bound-free and free-free contributions to the x-ray scattering spectrum.

IV. WARM DENSE BERYLLIUM

We now turn our attention to the WDM x-ray scattering experiment of Ref. [4]. In that experiment 6.2-keV x rays were scattered from warm dense beryllium and collected at 25° and 90°. From the 90° measurements the average free electron density of the plasma was determined to be $\bar{n}_e^0 = 7.5 \times 10^{23}$ cm^{-3} ($\pm$7%), corresponding roughly to 3 times the normal density (5.55 g/cm^3), with $\bar{Z} = 2$ ($\pm$25%) and an ion temperature of 13 eV ($\pm$10%). From the 25° measurements the average free electron density the plasma was determined to be $\bar{n}_e^0 = 7.5 \times 10^{23}$ cm^{-3} ($\pm$6%), while the electron temperature was found to be 13 ± 3 eV [4], both in excellent agreement with the 90° data. The source spectrum was measured and is given in Ref. [4].

In Fig. 2 we show the k dependence of the elastic component of Eq. (2) for a temperature of 13 eV and mass density of 5.55 g/cm^3 as calculated with our model using the Dirac exchange potential. For this density and temperature, the model predicts that $\bar{n}_e^0 = 7.46 \times 10^{23}$ cm^{-3}, $\bar{Z} = 2.01$, and finds one bound state with a binding energy of -69.5 eV, with an occupation of 1.99, in excellent agreement with the values of Ref. [4]. From the figure we see that as $k \to 0$ $f_I(k)$ and $q(k)$ go to the number of bound and free electrons per ion, respectively. The experiment probes the region where the ion-ion structure factor $S_{ii}(k)$ is rising with k. This is confirmed by a quantum molecular dynamics calculation [25] which agrees well with the prediction of our model (Fig. 2). For the smaller angle both $f_I(k)$ and $q(k)$ are significant, while for 90° the model

[3]This would be equal to the Fermi energy if the continuum electrons were truly free.

[4]This is simply $\frac{3}{2}$ times the Dirac exchange [Eq. (9)].

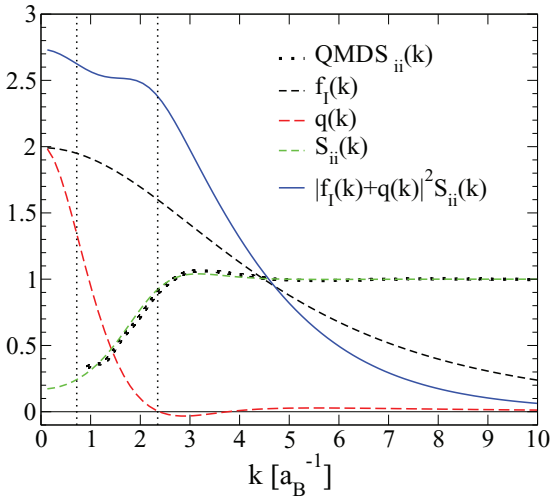

FIG. 2. (Color online) k dependence of the elastic component of the structure factor for beryllium at 13 eV and 5.55 g/cm^3 as calculated with the WDM model of Ref. [12]. A quantum molecular dynamics calculation of $S_{ii}(k)$ is also shown [25]. The vertical dotted lines correspond the k values of the experiment at 25° ($k = 0.720a_B^{-1}$) and 90° ($k = 2.35a_B^{-1}$). These correspond to scattering parameters of $\alpha = 1.73$ and 0.53, respectively. The quantities shown on the vertical axis are dimensionless.

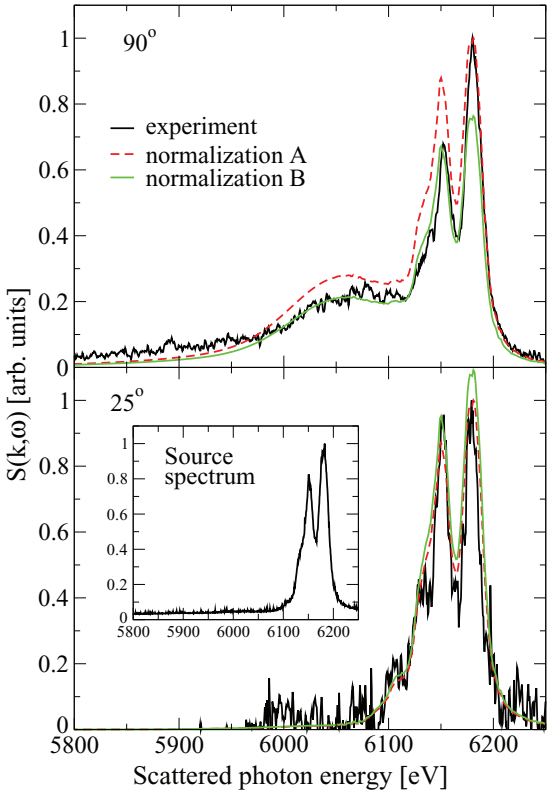

FIG. 3. (Color online) Comparison of synthetic spectra to an x-ray scattering experiment on warm dense beryllium [4] assuming a temperature of 13 eV and density of 5.55 g/cm^3 (threefold compression). The experimental spectra are in arbitrary units. The two theoretical curves show the same calculation normalized to match the magnitude of either the right-hand peak (normalization A) or the left-hand peak (normalization B). The inset shows the spectrum of the incident x-ray source.

predicts that $q(k)$ is negligible compared to $f_I(k)$. We thus expect a partial cancellation of the variations in $S_{ii}(k)$ and of $q(k)$ between these two scattering angles, as shown by the relatively flat behavior of the elastic peak between the two experimental k values.

In Fig. 3 we compare directly to the experimental data for both scattering angles. The source spectrum which we used to convolve our theoretical spectrum is shown in the inset. The experimental data are arbitrarily normalized, and we show the same theoretical x-ray spectrum scaled by two different choices of normalization. First, consider the case where we have normalized to the height of the right-hand peak of the experimental elastic feature (labeled "normalization A" in the figure). For the 90° spectrum, this peak is recovered well but the spectrum disagrees with the experiment everywhere else. When the theoretical spectrum is normalized to the left-hand peak in Fig. 3 ("normalization B") there is good agreement with the measured inelastic feature for 90° but it no longer matches the right-hand peak of the elastic feature. At a scattering angle of 25° (lower panel of Fig. 3), both normalizations match the data reasonably well.

Comparing the source spectrum (inset in Fig. 3) to the 90° data, we see that the right-hand peak has become stronger in the scattered spectrum relative to the left-hand peak. As noted earlier, in the Chihara formulation [Eq. (2)] the elastic feature of the scattered spectrum simply reflects the shape of the source spectrum. On the other hand, the inelastic features (bound-free and free-free) are down-shifted in energy from the incident energy (6.2 keV) and will contribute more to the height of the left-hand peak than to the right-hand peak (Fig. 4). Thus, in the scattered doublet, the left-hand peak can only become stronger with respect to the right-hand peak, which is the opposite of what is observed in the 90° spectrum. The observed peak ratio in the 90° data cannot be reconciled on theoretical grounds with the peak ratio in the source spectrum provided. The reason that the 90° data is not well matched using normalization A could be due either to source variability or to variations in the intensity of the optically thick resonance line at 6181 eV as the viewing angle (and thus line-of-sight depth) between the source and the sample is changed. Given the ambiguity in the scaling of the model spectrum for this experiment, we consider the agreement with the data to be good.

In Fig. 4 we show the components of the calculated dynamical structure factor, using normalization B. For both angles, the two approximations for the free-free component, the RPA and the BM approximation, are very close to each other. For 90° the bound-free contribution becomes apparent but remains relatively small. However, the long-range tail does not recover the experiment well, in contrast to the excellent agreement we found for solid beryllium (Fig. 1). In the 25° spectrum the bound-free contribution is negligible. The free-free term is shifted to lower energy transfer, as expected from the change in the Compton shift $\omega_0 - \omega_1 \sim E_C = k^2/2 = 2k_0^2 \sin^2\theta/2$ and, while it is not small, it is largely masked by the broad elastic peak produced by the double-peaked source spectrum. At this angle the scattering is strongly collective ($\alpha = 1.73$) and the (unconvolved) RPA

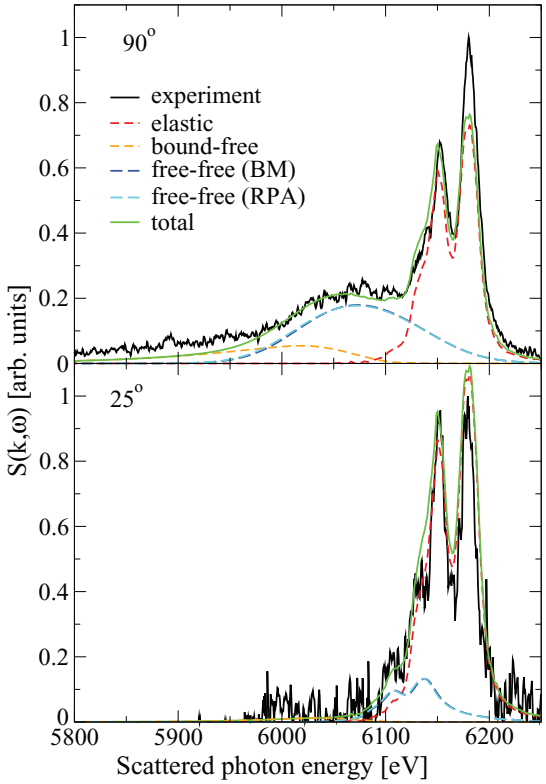

FIG. 4. (Color online) Same as Fig. 3 for warm dense Be but showing the separate contributions to the spectrum. Both the RPA and the Born-Mermin calculations of the free-free contribution are shown. The curve labeled "total" uses the BM result for the free-free component. The theoretical curves correspond to normalization B of Fig. 3.

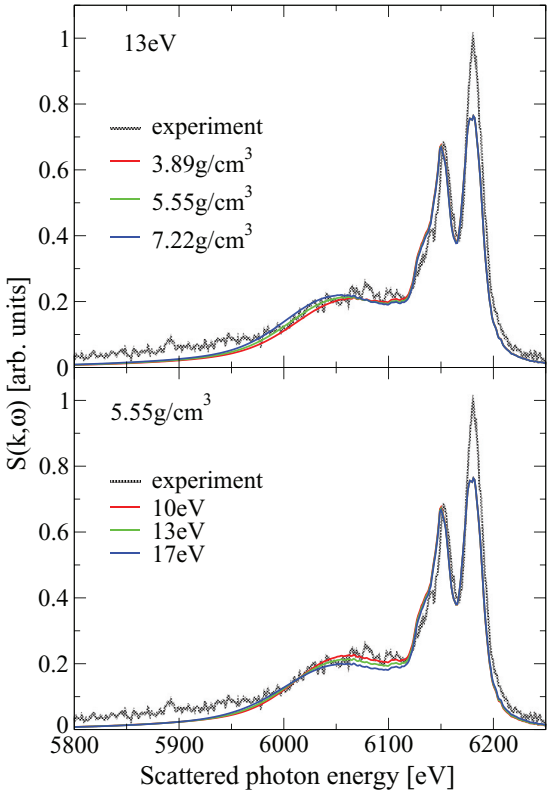

FIG. 5. (Color online) Sensitivity of the calculated x-ray scattering spectrum to variations in density and temperature for the experiment on warm dense beryllium with $\theta = 90^\circ$ [4]. The variations shown correspond to ±30% about the nominal values. The theoretical curves correspond to normalization B of Fig. 3. In the top panel the upper line corresponds to the highest density, and the lowest line to the lowest density. In the bottom panel the upper line corresponds to the lowest temperature, and the lowest line to the highest temperature.

(and the BM approximation) probably overestimate $S_{ee}(k,\omega)$ by ∼50% [25].

In Fig. 5 we explore the sensitivity of the theoretical spectrum (at 90°) to the assumed plasma conditions. Based on the reported uncertainties, we consider variations of ±30% in density and temperature about the nominal values of 5.55 g/cm^3 and 13 eV, again assuming normalization B. For both density and temperature variations we find a rather small effect on the spectrum because the ion charge $\bar{Z}$ and the bound state properties of Be are nearly constant over this range. The variations in the spectrum are even smaller for the scattering angle of 25° as the bound-free and free-free contributions are much reduced compared to the elastic peak (not shown). Noise in the data and uncertainty in the source spectrum (Fig. 3) can easily mask these small changes. To maximize the utility of x-ray scattering experiments as tools to extract the temperature and density of warm dense plasmas, it is therefore essential to use a source spectrum that is narrow compared to the Compton shift and that is well characterized for each experimental shot.

Finally, all calculations in Figs. 2 to 5 use the Dirac exchange potential. We have repeated the calculations with the Slater exchange potential and find only relatively small differences. However, due to the ambiguity in the normalization of the data, these differences are not significant and we do not show these results.

V. WARM DENSE ALUMINUM

In the experiment of Ref. [6], 17.9-keV x rays were scattered from a warm dense aluminum target. Spectra were presented for $\theta = 69^\circ$ and 111° in absolute units and the source spectra was determined to have a Gaussian shape (325-eV FWHM). The conditions of the target are reported to be 10 eV and 8.1 g/cm^3, corresponding to a threefold compression, while the average ionization was determined to be $\bar{Z} = 3$. Using the Dirac exchange functional, our model [12] predicts three bound states for these conditions, the $1s$, $2s$, and $2p$ states, having energies of −1.47 keV, −75.7 eV, and −38.3 eV, respectively. The average ionization is found to be $\bar{Z} = 3.04$, corresponding to an electron density of $\bar{n}_e^0 = 5.5 \times 10^{23}$ cm^{-3}. The k dependence of the elastic feature is shown in Fig. 6. The ion-ion structure factor $S_{ii}(k)$ as calculated from our model shows only a small first peak, indicative of a modestly coupled plasma and is in excellent agreement with a quantum molecular dynamics simulation for the same conditions. For both angles, the experimental k value is well within the asymptotic regime where $S_{ii}(k) = 1$. On the other hand, the screening density form factor $q(k)$ is negligible compared to the ion form factor $f_I(k)$. Thus the change in magnitude of the elastic feature between the two scattering angles is entirely dominated by the

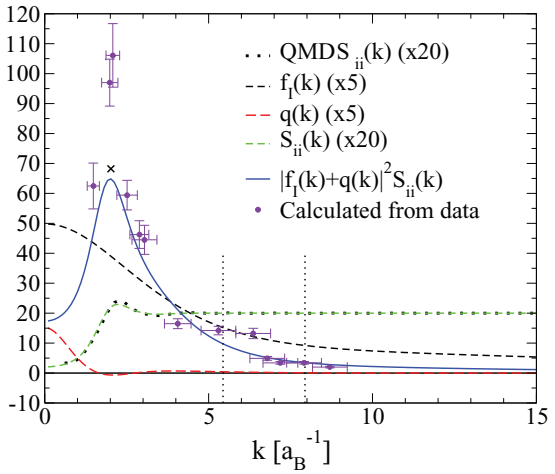

FIG. 6. (Color online) k dependence of the elastic component of the structure factor for aluminum at 10 eV and 8.1 g/cm^3 as calculated with the WDM model of Ref. [12]. The dotted vertical lines correspond the the k values of the experiment [6] at 69° ($k = 5.44a_B^{-1}$) and 111° ($k = 7.94a_B^{-1}$). The $S_{ii}(k)$ obtained from a quantum molecular dynamics calculation [29] is also shown for comparison. The small cross indicates the change in the position of the peak (solid curve) that results from replacing $S_{ii}(k)$ from our model with that of the QMD calculation in the calculation of the elastic feature. Points with error bars are $|f_I(k) + q(k)|^2 S_{ii}(k)$ extracted from the experiment of Ref. [6]. For clarity, $f_I(k)$, $q(k)$, and $S_{ii}(k)$ have been scaled as indicated in the legend. The quantities on the vertical axis are dimensionless.

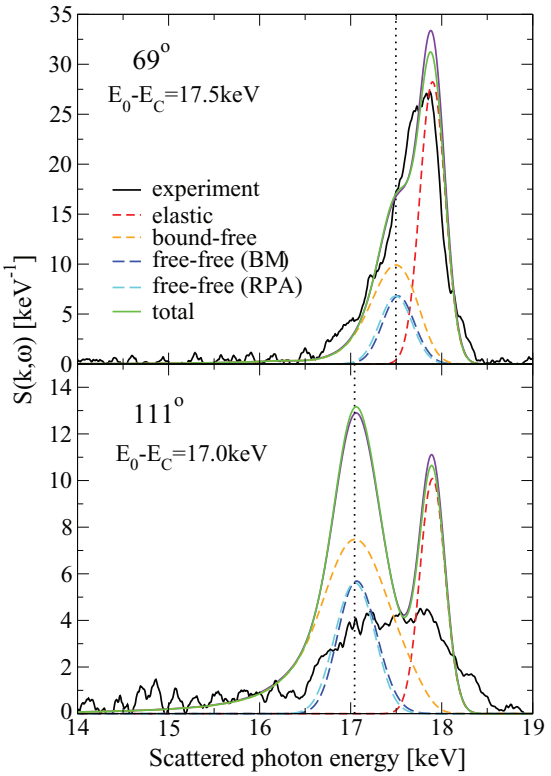

FIG. 7. (Color online) Comparison of synthetic x-ray scattering spectra to an experiment on warm dense aluminum [6], assuming a temperature of 10 eV and density of 8.1 g/cm^3 (threefold compression). The vertical dotted line shows the position of the Compton edge. The curve labeled "total" uses the Born-Mermin (BM) calculation of the free-free component. All theoretical curves shown use the Dirac exchange potential except the solid purple (dark gray) line, which is the total spectrum obtained when using the Slater exchange potential. It overlaps the Dirac exchange calculation almost everywhere.

change in $f_I(k)$. The scattering parameter is $\alpha = 0.22$ at 69° and 0.11 at 111°. We expect the RPA to perform rather well in this strongly noncollective regime.

In Fig. 7 we show our calculations of the x-ray scattering spectra compared to the experimental data [6] for both angles, along with each of the components contributing to the total spectrum. Since the data are reported in absolute units, we can compare directly with our calculations after convolving with the Gaussian profile of the incident x-ray probe beam without any scaling. In the top panel ($\theta = 69°$) the agreement is reasonably good. As expected, the inelastic free-free component peaks near the position of the Compton edge, which is down-shifted from the elastic peak by $E_C = k^2/2$, as indicated in the figure. The RPA and BM approximations for the free-free component are very close to each other under these conditions, as was found for warm dense beryllium (Fig. 4). The bound-free contribution also peaks near the Compton edge in this experiment, with the result that it cannot be distinguished from the free-free scattering. This free-free like behavior of the bound-free contribution is explained by the incident photon energy being much larger than the binding energy of the electrons, essentially scattering them as if they were free. A similar calculation of the bound-free contribution is presented in Ref. [30]. Also shown is the total spectrum calculated with the Slater exchange potential, which has a small effect (∼5%) on the peak heights compared to the calculation with Dirac exchange. This result gives us an indication of the magnitude and type of effect the exchange (and correlation) potential has on x-ray scattering spectra in WDM experiments.

In contrast to the good agreement with the 69° spectrum, the calculated spectrum and the data differ remarkably for the scattering angle of 111° (Fig. 7, bottom panel). To zeroth order, both the calculated spectrum and the data show that the inelastic peak is of similar amplitude to the elastic peak. The larger Compton shift at this angle clearly separates the elastic and inelastic features in the model spectrum, resulting in a double-peaked structure. On the other hand, the data show a single broad peak whose width is roughly comparable to that of our calculation but with only about one-third the amplitude.

In the data, the elastic peak is ∼7 times smaller than at 69°, while our model predicts a decrease by a factor of 3. This is significant since no normalization is applied in this comparison as the data are reported in absolute units. Fortunately, this case lends itself to a deeper analysis. As shown in Fig. 6, both spectra correspond to fairly large values of k where our model predicts that $S_{ii}(k) = 1$ and $q(k) \approx 0$. Thus the model predicts that the variation in the height of the elastic peak at 17.9 keV will come solely from the change in $f_I(k)$, the form factor of the bound electrons [Eq. (2)]. We have considered each

of these contributions to the elastic peak. Our ionic structure factor for this plasma is in excellent agreement with that from a quantum molecular dynamics simulation [29] (Fig. 6). The form factor $q(k)$ represents the cloud of screening electrons, whose radial distribution around an ion can depend sensitively on assumptions in the WDM model. The experimental plasma is fairly degenerate (the Fermi energy is 24.5 eV and $T =$ 10 eV). A simple Yukawa model of screening with a screening wave vector $k_{\rm scr} = 1.19a_B^{-1}$ [Eq. (5)] confirms that $q(k)$ should be very small since $k \gg k_{\rm scr}$ for scattering angles of 69° and 111°, regardless of how the screening is modeled.[5] The ion form factor $f_I(k)$ is determined by the wave functions of the three bound states. We have verified that a nearly identical $f_I(k)$ is obtained from an independent average atom model (MUZE) [31,32]. A Dirac-Fock-Slater calculation [33] of the core electron density of an isolated Al^{3+} ion shows only minute differences from our $f_I(k)$. Having thus checked each component of the elastic feature, we find that no realistic WDM model would predict the experimentally observed magnitude for the elastic feature at 111°. One mechanism that would achieve a reduction in the elastic peak is if the source spectrum was significantly broader than reported or non-Gaussian.

The free-free component is insensitive to the choice of approximation as both the RPA and the BM approximation give nearly identical results (Fig. 7). These two scattering angles correspond to the strongly noncollective regime ($\alpha = 0.11$ and 0.22) and we expect the RPA to be a good approximation to $S_{ee}(k,\omega)$ [25]. This experiment is in the limit where $k > 2k_F$ ($k_F = 1.34$ is the Fermi wave vector), where the static structure factor $S_{ee}(k) = \int S_{ee}(k,\omega)\, d\omega \to 1$. We have checked that the frequency integral of the free-free component changes little between these two scattering angles, as is confirmed by Fig. 7. For the bound-free component we have verified that an independent calculation using the MUZE average atom model gives nearly identical results.

There seems to be no room in our model to account for the difference between the modeled and observed spectra at 111°, particularly considering the good agreement we find with the 69° spectrum. Finally, we have checked the sensitivity of the spectra to density and temperature variations (±30%) and found an almost negligible dependence for both angles. This detailed discussion shows that in this case, no realistic model of the plasma would give properties that differ much from those calculated with our model of WDM.

From a theoretical point of view, the discrepancy could be attributed to the Chihara decomposition of the scattered spectrum into distinct elastic, bound-free, and free-free contributions [Eq. (2)]. This formalism relies primarily on the assumption that the bound states are well separated from the continuum. We found that under these experimental conditions, the most weakly bound electrons of the Al ion have a binding energy of $|E_{2p}| = 38.3$ eV, well above the temperature of the plasma (10 eV) and the Fermi energy (24.5 eV). Inspection of the bound electron density profile shows that only a very small fraction leaks outside of the ion sphere. Under these circumstances the Chihara formalism should be valid.

Figure 6 shows the amplitude of the elastic peak $|f_I(k) + q(k)|S_{ii}(k)$ as a function of the wave vector k. The data shown are extracted from spectra taken at 13 scattering angles, after modeling and removing the bound-free and free-free contributions [Eq. (2)]. For small k values, the latter are relatively small and the entire scattered line can be attributed to the elastic peak. Experimentally, a sharp maximum of 106 at $k = 2.1a_B^{-1}$ is found while our model predicts a peak of 65 at $k = 2.0a_B^{-1}$. Apart from the two points near the peak our model generally agrees well with the values extracted from the data. The small black cross in the figure indicates the maximum peak height that would occur if $S_{ii}(k)$ from the QMD simulation [29] was used instead of that calculated from our model. As can be seen from the figure, the difference is small, with the peak height changing to 68, insufficient to account for the large difference seen.

In Ref. [6], the larger peak was reproduced with a model including ion-ion correlations described with a combination of a Yukawa potential and a short-range repulsion between ions due to bound electrons; the latter being essential to match the height of the peak. On the other hand, our model of WDM, which also accounts for ion-ion correlations and strongly nonlinear screening based on the electronic wave functions and self-consistently generates the ion-ion potential, predicts a maximum in the elastic peak that is much lower. The fact that our $S_{ii}(k)$ agrees very well with a QMD simulation (Fig. 6) for this Al plasma shows that our ion-ion potential describes the system well without introducing an *ad hoc* short-range

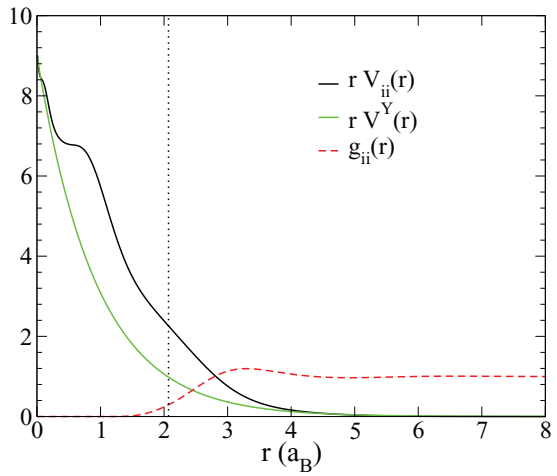

FIG. 8. (Color online) Comparison of ion-ion potentials used in calculations of the structure factor $S_{ii}(k)$ for warm dense Al at 10 eV and 8.1 g/cm^3. For clarity, the product $rV(r)$ is shown. The potential calculated with a self-consistent model of WDM [12,13] [$V_{ii}(r)$, black] is affected by the shell structure of the ion and is more repulsive than a Yukawa potential with screening wave vector $k_{\rm scr} = 1.07a_B^{-1}$ [18,21] [$V^Y(r)$, green (light gray)]. The dashed curve shows the pair distribution function $g(r)$ computed with the former potential. The ion sphere radius is indicated by the vertical dotted line. The two potentials are substantially different in a range of radii where $g(r)$ is not small.

[5]The same reasoning applied to the warm dense Be case of Sec. IV confirms that $q(k)$ becomes very small where expected and that the experiment probes k values small enough for the screening model to matter.

repulsion. In fact, the orthogonality of the electronic states obtained by solving the Schrödinger equation [12] tends to push the free electrons out of the core of bound electrons and thus results in weaker screening than the Yukawa screening of a point ion of the same charge. The Yukawa potential is considerably more attractive than our ion-ion potential in a range of separations of significant correlations in the fluid ($r \sim 2 - 4a_B$). Figure 8 shows that a repulsive term would have to be added to a Yukawa potential to reproduce the pair distribution function and structure factor of a QMD simulation [6,34]. Such significant divergences between models of WDM can be resolved partially with comparisons with *ab initio* simulations that rely on fewer approximations. However, this cannot replace well-controlled experiments with parameters chosen to highlight the relevant physics.

VI. PREDICTION FOR A WARM DENSE BERYLLIUM EXPERIMENT

In this spirit, we consider a hypothetical experiment with beryllium that combines the WDM conditions of Ref. [4] with the x-ray probe used in the cold Be experiment [7]. The latter is mainly characterized by a very high intensity beam with a very narrow spectral distribution and a long duration that lead to high signal-to-noise data and high spectral resolution. In Fig. 9 we show our prediction for the spectra from a Be target at 13 eV and 5.55 g/cm^3 for the set of angles used in Ref. [7]. For these conditions $\bar{Z} = 2.01$. This can be compared directly to Fig. 1. The differences are due only to temperature and density effects as predicted by our model. We have omitted the elastic peak from the spectrum in Fig. 9, which would appear as a very narrow feature at $\omega = 0$.

Compared to the cold Be experiment, the peak of the spectrum is reduced by a factor of $\sim 2/3$ and the bound-free edge is no longer sharp. The softening of the bound-free edge is due to the smearing of the Fermi distribution for the continuum electrons that occurs at higher temperatures and is therefore a consequence of accounting for the occupation of the final state in the bound-free calculation. The free-free component is also broadened and, consequently, of lower amplitude to give the same $S_{ee}(k) = \int S_{ee}(k,\omega)\, d\omega$. Again, this is a result of the broadening of the Fermi edge or, equivalently, of the broader momentum distribution of electrons at finite T for a given electron density. The broadening occurs over a range of $\hbar\omega \sim kT$, typically of the order of 10 eV in WDM experiments. This explains to some extent why the RPA appears to be an accurate description of the free-free feature in WDM experiments but not in the cold Be experiment. For the cold Be experiment [7] (Fig. 1) is was found that the RPA was too large in magnitude at its peak and too narrow at its base. Broadening due to temperature corrects this inadequacy somewhat. Furthermore, the broad source spectra typically used in WDM x-ray scattering experiments [4,6] smooths the spectrum over $\sim 10^2$ eV and further tends to mask any shortcomings of the RPA. Our calculation of the free-free contribution with the BM approximation is essentially identical to the RPA result in this example. For completeness we also show in Fig. 9 the result using the Slater exchange potential to model the electrons. As we found for the cold Be experiment, the result is mostly indistinguishable from the calculation with Dirac exchange except near the bound-free edge and then only for the smaller k values.

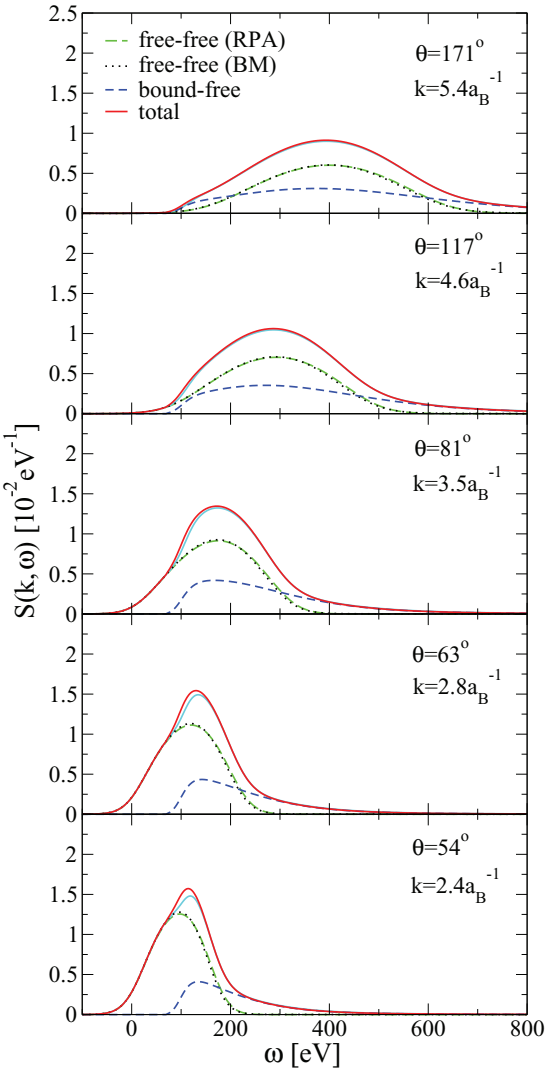

FIG. 9. (Color online) Theoretical spectra for warm dense beryllium with the same conditions as in the warm dense Be experiment (5.55 g/cm^3 and 13 eV; Figs. 3 and 4) and the same k vectors and x-ray probe profile as for the experiment on cold Be [7] (Fig. 1). The curves are shown for calculations with the Dirac exchange functional. The solid cyan (light gray) line is the result using Slater exchange and is mostly indistinguishable from the Dirac exchange calculation except near the bound-free threshold. For ease of comparison, we show this figure with the same frequency axis as in Fig. 1, which is reversed from that of Figs. 3–5 and 4.

VII. FEATURES IN THE BOUND-FREE SPECTRUM

In the Be case discussed in the previous section (Fig. 9), the bound-free contribution to the scattered spectrum is smooth. In higher Z elements, the bound-free term is the sum of contributions from multiple bound states and can show several bound-free edges. Average atom models predict that inelastic scattering off of bound electrons can also produce sharp peaks for transitions to resonant continuum states [35]. Our WDM model predicts multiple bound-free edges and resonant peaks

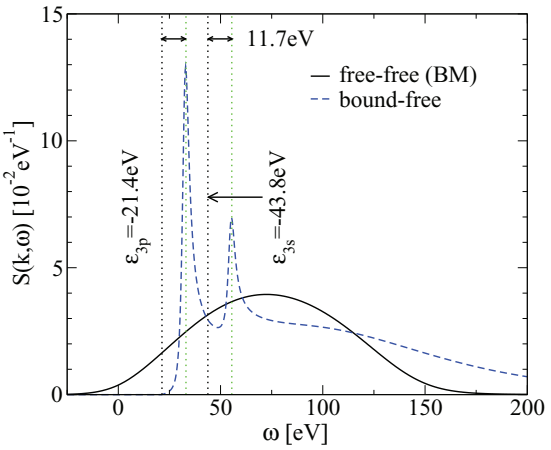

FIG. 10. (Color online) Theoretical bound-free and free-free contributions to the x-ray scattering spectrum of warm dense titanium at 5 eV and 4.51 g/cm^3. The probe beam has an energy of $\omega_0 = 4.750$ keV and the angle is 130°. The spectrum is not convolved with a source spectrum. The black vertical dotted lines mark the energies of the $3s$ and $3p$ bound states. The green (light gray) vertical dotted lines mark these bound state energies plus the energy of the $3d$ resonant state (11.7 eV). Note that the frequency axis is reversed, as in Figs. 1 and 9.

in x-ray scattering spectra as well. This is expected since we apply the same formalism to calculate the bound-free scattering as Ref. [35] and our WDM model naturally accounts for all bounds states and continuum resonances.

Figure 10 shows an x-ray scattering spectrum for titanium at 5 eV and 4.51 g/cm^3 (solid density), with a probe beam of 4.750 keV and a scattering angle of 130° (see Ref. [35] for a similar calculation). The bound-free spectrum contains contributions due to photo-ionization of the $3s$ and $3p$ bound states, with binding energies of -43.8 eV and -21.4 eV, respectively. The most notable features are due to transitions from these bound states to a $3d$ continuum resonance, located at a positive energy $\sim$11.7 eV. Because average atom models impose spherical symmetry, they predict resonances that are too strong and narrow. In a disordered system such as a plasma, resonances are still present but are broadened significantly [36]. Nonetheless, Fig. 10 shows that it is possible to probe the structure of resonant continuum states in WDM with x-ray scattering experiments and test model predictions that can affect transport properties. As can be seen in the figure, such measurement requires a probe beam with a spectral distribution that is narrow enough to reveal the structure in the spectrum of the order of 5 eV. This is especially important since the elastic peak at $\omega_1 - \omega_0 = 0$ is very strong and its broadening into the 20–70 eV range would overwhelm the bound-free signal.

VIII. CONCLUSIONS

We have presented calculations of x-ray scattering spectra for WDM using the Chihara formalism for scattering [15] and a new model for the properties of dense plasmas [12]. The model has no adjustable parameters and unique predictions of scattering spectra are obtained given the element's nuclear charge and atomic mass, the mass density and temperature, and experimental parameters. Variants of the model can be produced with different choices of approximations such as the exchange and correlation potential. This model of WDM has been applied successfully to the calculation of pair distribution functions for elements from hydrogen to tungsten over a wide range of conditions [12,13,37]. The Chihara formalism is implemented by using quantities directly calculated from our WDM model for the elastic feature, the approach of Ref. [35] for the bound-free contribution, which uses the bound and continuum wave functions from our WDM model, and either the RPA or the Born-Mermin approximation for the free-free component.

A comparison of the modeled x-ray scattering spectra to a series of high-resolution, high-signal-to-noise-ratio experimental spectra from a room-temperature, solid beryllium target reveals systematic deviations of moderate magnitude that can be attributed to approximations in our model. Specifically, one limitation is the use of the DFT to compute electronic wave functions, which underestimates the binding energies, and the other is the RPA, which approximates the free-free scattering reasonably well in the regime of noncollective scattering but not as successfully as more advanced, zero-temperature theories [7]. This comparison provides a quantification of the errors introduced by the approximations in the WDM model and by the model for the x-ray scattering. The generally good agreement with this exacting data validates our approach and justifies its application to x-ray scattering spectra of WDM targets. Compared to the cold Be experiment conducted under ambient conditions, WDM experiments are technically quite challenging and the resulting spectra have lower signal-to-noise ratios and lower spectral resolution and are not as well controlled.

We analyzed the x-ray scattering spectra acquired in two WDM experiments. For the Be experiment [4], we found good agreement with the spectra obtained at two scattering angles. However, there is some inconsistency between the 90° spectrum and the probe spectrum, resulting in an ambiguity in the analysis that is significant. The sensitivity of the spectrum to variations in density and temperature of $\pm 30\%$ is small, comparable to the noise level, and easily masked by the uncertainty in the spectral distribution of the probe x rays. We are unable to match the long-range tail of the 90° spectrum that arises from the bound-free contribution, in contrast to the good agreement found with the cold Be experiment for this feature.

On the other hand, the free-free component of the spectra agrees well with the experiments at warm dense conditions while we found systematic deviations of the RPA with the cold Be data. However, shortcomings in the RPA could be masked by the broad source spectrum used in the experiment [4,6] which tends to correct for the deviations from the cold Be data. Moreover, this apparent validity of the RPA is weakened by other points of disagreements with the data.

For the warm dense aluminum experiment [6] we find good agreement with the data at one scattering angle (69°) and strong disagreement with the other (111°). In particular, the elastic peak and the sum of the bound-free and free-free contributions produce a strong double-peaked spectrum while only a broad, flat feature is observed. We have argued that this disagreement is difficult to understand from a theoretical perspective as our

result is supported by several independent checks and simple physics arguments.

Finally, we have isolated the effects of warm dense target conditions by comparing the theoretical spectra for the cold Be experiment to that of warm dense Be for the same x-ray probe. Temperature effects reveal themselves primarily via a blurring of the Fermi edge, resulting in a smearing out of the bound-free and free-free features which is most noticeable near the bound-free threshold.

WDM is widely acknowledged as being challenging to model and much theoretical development is needed to fill large gaps in our understanding of the physics of WDM and to reliably model natural and laboratory systems where WDM occurs [9]. Experiments have a crucial role to play in evaluating competing models and in measuring the properties of WDM directly. X-ray scattering arises from a host of atomic-scale and collective phenomena. Such experiments have the potential to probe many microscopic features of warm dense plasmas, such as the number and energies of bound states; continuum resonances; the response of a correlated, partially degenerate electron fluid (beyond the RPA); collective phenomena; electron screening in strongly nonlinear regimes; ion-ion correlations; and pressure ionization. These exciting prospects as well as the ability to discriminate between models of WDM [8,16,18,21,38] and advances in the theory of x-ray scattering [15] in WDM are not yet realized experimentally. The cold Be experiment and its modeling [7,8,26], as well as the synthetic spectra presented here show that such investigations of WDM will be enabled by data with much higher signal-to-noise and higher spectral resolution than have been achieved so far for WDM targets. We have also found that well-characterized probe beams are essential for a meaningful analysis of x-ray scattering spectra. The bright, narrow x rays available on modern XFELs and even the narrow Heβ lines that accompany Heα emission from laser plasmas could provide much cleaner data that would enable more stringent tests of theory. Finally, models of WDM and the theory of x-ray scattering in dense plasmas are constrained most effectively by experiments where parameters such as the temperature and density are measured independently from the spectrum.

ACKNOWLEDGMENTS

We thank H. J. Lee and T. Ma for providing their experimental data and for useful discussions, J. D. Kress for providing the quantum molecular dynamics simulation of aluminum, and K.-U. Plagemann for that of beryllium. We are grateful to J. F. Benage and K. Falk for valuable discussions on WDM experiments and to C. F. Fontes for providing the Dirac-Fock-Slater calculation. This work was performed under the auspices of the United States Department of Energy under Contract No. DE-AC52-06NA25396.

[1] S. H. Glenzer, G. Gregori, R. W. Lee, F. J. Rogers, S. W. Pollaine, and O. L. Landen, Phys. Rev. Lett. **90**, 175002 (2003).
[2] E. G. Saiz *et al*., Nat. Phys. **4**, 940 (2008).
[3] A. L. Kritcher *et al*., Science **322**, 69 (2008).
[4] H. J. Lee *et al*., Phys. Rev. Lett. **102**, 115001 (2009).
[5] S. P. Regan *et al*., Phys. Rev. Lett. **109**, 265003 (2012).
[6] T. Ma, T. Döppner, R. W. Falcone, L. Fletcher, C. Fortmann, D. O. Gericke, O. L. Landen, H. J. Lee, A. Pak, J. Vorberger, K. Wünsch, and S. H. Glenzer, Phys. Rev. Lett. **110**, 065001 (2013).
[7] B. A. Mattern, G. T. Seidler, J. J. Kas, J. I. Pacold, and J. J. Rehr, Phys. Rev. B **85**, 115135 (2012).
[8] B. A. Mattern and G. T. Seidler, Phys. Plasmas **20**, 022706 (2013).
[9] Report of ReNew workshop. *Basic research needs for high energy density laboratory physics*. U.S. Department of Energy, (2009) http://science.energy.gov/~/media/fes/pdf/workshop-reports/hedlp_brn_workshop_report_oct_2010.pdf.
[10] G. Chabrier and E. Schatzmann, *IAU Colloquium 147, The Equation of State in Astrophysics* (Cambridge University Press, Cambridge, 1994).
[11] B. A. Hammel, S. W. Haan, D. S. Clark, M. J. Edwards, S. H. Langer, M. M. Marinak, and M. V. Patel, High Energy Dens. Phys. **6**, 171 (2010).
[12] C. E. Starrett and D. Saumon, Phys. Rev. E **87**, 013104 (2013).
[13] C. E. Starrett and D. Saumon, High Energy Dens. Phys. **10**, 35 (2014).
[14] C. E. Starrett and D. Saumon, Phys. Rev. E **85**, 026403 (2012).
[15] J. Chihara, J. Phys.: Condens. Matte **12**, 231 (2000).
[16] W. R. Johnson, J. Nilsen, and K. T. Cheng, Phys. Rev. E **86**, 036410 (2012).
[17] N. R. Arista and W. Brandt, Phys. Rev. A **29**, 1471 (1984).
[18] S. H. Glenzer and R. Redmer, Rev. Mod. Phys **81**, 1625 (2009).
[19] H. Reinholz, R. Redmer, G. Röpke, and A. Wierling, Phys. Rev. E **62**, 5648 (2000).
[20] N. D. Mermin, Phys. Rev. B **1**, 2362 (1970).
[21] G. Gregori, S. H. Glenzer, W. Rozmus, R. W. Lee, and O. L. Landen, Phys. Rev. E **67**, 026412 (2003).
[22] M. S. Murillo, Phys. Rev. E **81**, 036403 (2010).
[23] G. Gregori, A. Ravasio, A. Höll, S. H. Glenzer, and S. J. Rose, High Energy Dens. Phys. **3**, 99 (2007).
[24] E. M. Lifshitz and L. P. Pitaevskii, *Course of Theoretical Physics, Vol 10: Physical Kinetics* (Pergamon, Oxford, 1981).
[25] K.-U. Plagemann, P. Sperling, R. Thiele, M. P. Desjarlais, C. Fortmann, T. Döppner, H. J. Lee, S. H. Glenzer, and R. Redmer, New J. Phys. **14**, 055020 (2012).
[26] B. A. Mattern, G. T. Seidler, and J. J. Kas (2013), arXiv:1308.2990.
[27] P. A. M. Dirac, Proc. Camb. Phil. Soc **26**, 376 (1930).
[28] J. C. Slater, Phys. Rev. **81**, 385 (1951).
[29] J. D. Kress and L. A. Collins (private communication, 2012).
[30] J. Nilsen, W. R. Johnson, and K. T. Cheng, Proc. SPIE **8849**, 884915 (2013).
[31] J. E. Bailey, T. Ao, E. Harding, S. B. Hansen, M. P. Desjarlais, R. W. Lemke, G. A. Rochau, J. Reneker, and D. Romeror. Sandia Rep., 2012-7998, (2012).

[32] S. B. Hansen, A. Ya. Faenov, T. A. Pikuz, K. B. Fournier, R. Shepherd, H. Chen, K. Widmann, S. C. Wilks, Y. Ping, H. K. Chung, A. Niles, J. R. Hunter, G. Dyer, and T. Ditmire, Phys. Rev. E **72**, 036408 (2005).

[33] D. H. Sampson, H. L. Zhang, and C. F. Fontes, Phys. Rep. **477**, 111 (2009).

[34] K. Wünsch, J. Vorberger, and D. O. Gericke, Phys. Rev. E **79**, 010201(R) (2009).

[35] W. R. Johnson, J. Nilsen, and K. T. Cheng, High Energy Dens. Phys. **9**, 407 (2013).

[36] J. Clérouin, C. Starrett, P. Noiret, P. Renaudin, C. Blancard, and G. Faussurier, Contrib. Plasma Phys. **52**, 17 (2012).

[37] D. Saumon, C. E. Starrett, J. D. Kress, and J. Clerouin, High Energy Dens. Phys. **8**, 150 (2012).

[38] S. Sahoo, G. F. Gribakin, G. Shabbir Naz, J. Kohanoff, and D. Riley, Phys. Rev. E **77**, 046402 (2008).